Solubilized Amnion Membrane Hyaluronic Acid Hydrogel Accelerates Full-Thickness Wound Healing

SEAN V. MURPHY [ORCID],[a] ALEKSANDER SKARDAL,[a,b] LUJIE SONG,[c] KHIRY SUTTON,[a] REBECCA HAUG,[a] DAVID L. MACK,[d] JOHN JACKSON,[a] SHAY SOKER,[a,b] ANTHONY ATALA[a]

Key Words. Skin • Wound healing • Solubilized amnion membrane • Biomaterial • Hydrogel

[a]Wake Forest Institute for Regenerative Medicine, Wake Forest School of Medicine, Medical Center Boulevard, Winston-Salem, North Carolina, USA; [b]Virginia Tech-Wake Forest School of Biomedical Engineering and Sciences, Wake Forest School of Medicine, Medical Center Boulevard, Winston-Salem, North Carolina, USA; [c]Department of Urology, Shanghai Jiao Tong University Affiliated Sixth People's Hospital, Shanghai, People's Republic of China; [d]Department of Rehabilitation Medicine, Institute for Stem Cell and Regenerative Medicine, University of Washington, Seattle, Washington, USA

Correspondence: Sean Murphy, Ph.D., Wake Forest Institute for Regenerative Medicine, Wake Forest School of Medicine, Medical Center Boulevard, Winston-Salem, North Carolina 27157, USA. Telephone: 336-713-7277; e-mail: semurphy@wakehealth.edu; or Anthony Atala, M.D., Wake Forest Institute for Regenerative Medicine, Wake Forest School of Medicine, Medical Center Boulevard, Winston-Salem, North Carolina 27157, USA. Telephone: 336-716-5701; e-mail: aatala@wakehealth.edu

ABSTRACT

The early and effective treatment of wounds is vital to ensure proper wound closure and healing with appropriate functional and cosmetic outcomes. The use of human amnion membranes for wound care has been shown to be safe and effective. However, the difficulty in handling and placing thin sheets of membrane, and the high costs associated with the use of living cellularized tissue has limited the clinical application of amniotic membrane wound healing products. Here, we describe a novel amnion membrane-derived product, processed to result in a cell-free solution, while maintaining high concentrations of cell-derived cytokines and growth factors. The solubilized amnion membrane (SAM) combined with the carrier hyaluronic acid (HA) hydrogel (HA-SAM) is easy to produce, store, and apply to wounds. We demonstrated the efficacy of HA-SAM as a wound treatment using a full-thickness murine wound model. HA-SAM significantly accelerated wound closure through re-epithelialization and prevented wound contraction. HA-SAM-treated wounds had thicker regenerated skin, increased total number of blood vessels, and greater numbers of proliferating keratinocytes within the epidermis. Overall, this study confirms the efficacy of the amnion membrane as a wound treatment/dressing, and overcomes many of the limitations associated with using fresh, cryopreserved, or dehydrated tissue by providing a hydrogel delivery system for SAM. STEM CELLS TRANSLATIONAL MEDICINE 2017;6:2020–2032

SIGNIFICANCE STATEMENT

The early and effective treatment of wounds is vital to ensure proper wound closure and healing with appropriate functional and cosmetic outcomes. This study confirms the efficacy of the amnion membrane as a wound treatment/dressing, and overcomes many of the limitations associated with using fresh, cryopreserved, or dehydrated tissue.

INTRODUCTION

Chronic and acute full-thickness wounds affect over seven million patients in the U.S. Full-thickness skin injuries are a major source of mortality and morbidity, and include an estimated 500,000 civilian burns treated in the U.S. each year [1, 2]. Chronic, large, or nonhealing wounds are especially costly because they often require multiple treatments; for example, a single diabetic foot ulcer can cost approximately $50,000 to treat [3]. Due to the continuing need for better products that help in healing and preventing infection, the global wound care market is expected to reach USD 20.4 Billion by 2021 [4].

The early treatment and the proper coverage of wounds are vital steps in increasing the survivability of patients with extensive wounds. Patients respond best when rapid treatments are available that result in closure and protection of the wounds as fast as possible. The gold standard wound treatment, still used in the clinic, is an autologous split-thickness skin graft. However, the adequate coverage of wounds is often a challenge particularly when there is limited availability of healthy donor skin to harvest. Allografts are another option, but due to their allogeneic nature, require immunosuppressive drugs to prevent rejection of the graft [5]. These limitations have led to the development of noncellular polymer scaffolds, such as Integra and Biobrane. While these materials have been shown to improve wound healing [6, 7], they are expensive and do not provide optimal cosmetic outcomes. Thus, there is a need for a wound healing and tissue engineering product with high clinical efficiency, which does not require a cellular component, but retains the bioactivity of a biological treatment.

Amnion membranes have been successfully used for wound and reconstructive purposes since the early 20th century [8]. There have been many studies demonstrating the safety and efficacy of

human amnion for wound treatment and the use of amnion for skin burn management has been reported in over 200 clinical trials. The amnion has also found relatively widespread application as a wound covering, with treatment for diabetic neurovascular ulcers, venous stasis ulcers, and various types of postsurgical and posttraumatic wound dehiscence [9–13]. Some examples include the use of amnion as a wound covering for burn wounds treated with split thickness skin grafts [14], for children with partial-thickness facial burns [15], and various other clinical trials showing similar successes with various preparation and application methodologies [16–19]. These studies demonstrate that the use of amnion as a wound covering contributes to accelerated wound closure, reduced inflammation and scarring, reduced pain, and fewer infections.

For many clinical examples, a sheet of amnion is generally placed over the wound and held in place with sutures, glue, or additional bandaging. However, while the use of amnion in these clinical settings appears to be advantageous, it is a somewhat difficult material to incorporate into routine clinical use. Limitations included difficulty to handle the thin sheets without folding or tearing, and the requirement for sutures or adhesives to hold the membrane in place over the wound. Additionally, the processing, transportation and storage of the living cellularized tissue has limited clinical applications due to cost. To partially address these limitations, some groups have developed methods for cleaning, preparing, and dehydrating human amnion. In this form, the material is stable at room temperature, with a shelf life of up to 5 years. However, while multiple studies have shown that the dehydration of the amnion does not affect its efficacy as a wound treatment [20–24], there are still significant limitations in the delivery and application of this intact amnion to large or irregular shaped wounds. This includes in the majority of treatment cases where an amnion sheet does not conform to an irregular wound size or topology.

Recently, various hydrogel biomaterials have been explored for many applications in regenerative medicine, including as delivery vehicles for drugs, proteins, and living cells. Through a detailed hydrogel characterization study, our group identified a commercially available hyaluronic acid (HA)-based hydrogel with a range of properties that make it ideal for many regenerative medicine applications [25]. HA is a nonsulfated glycosaminoglycan [26, 27], which has been manipulated into various forms [28, 29], including a modular system consisting of thiolated HA, thiolated gelatin, and a polyethylene glycol diacrylate (PEGDA) cross-linker (commercially available as HyStem by ESI-BIO) [30, 31]. We have recently demonstrated that this modified HA-hydrogel functioned as an ideal carrier for the bioprinting of amniotic fluid stem cells directly into full-thickness excisional wounds [32]. These studies demonstrated that the HA hydrogel with encapsulated stem cells improved wound healing, even though the presence of cells within the wound was only transient. Our studies demonstrated the potential of HA hydrogel to function as a delivery vehicle that supported the release of stem cell-derived paracrine factors, thereby increasing their therapeutic effectiveness in wound healing.

In this reported study, we have developed a novel amnion membrane-derived product, processed to result in a cell-free solution, while maintaining high concentrations of cell-derived cytokines and growth factors. The solubilized amnion membrane (SAM) combined with the carrier HA hydrogel, results in an effective product that is easy to produce, store, and apply to wounds to accelerate wound closure and re-epithelialization.

MATERIALS AND METHODS

Preparation of Solubilized Amnion Membrane

Donated human placenta was collected and stored at 4°C for a maximum of 24 hours. The amnion membrane (avascular/inner) was manually dissected from the chorion membrane (vascular/outer). Any blood clots present were removed. The membrane was washed with 500–1,000 ml of sterile saline. Using sterile scissors and forceps, the amnion was cut into approximately 5×5 cm pieces. The amnion pieces were then transferred into a sterile 500 ml container and washed five times with 100 ml sterile saline. Pieces were then washed with 500 ml sterile water. The amnion pieces were transferred into 50 ml tubes. During transfer, the pieces were dragged along the edge of the 500 ml container in order to remove as much water as possible from each piece. Each 50 ml tube was filled to a maximum of 25 ml. The 50-ml tubes containing the amnion pieces were then kept at $-80°C$ for 12–24 hours. The lids of the 50 ml tubes were removed and replaced with sterile filter caps. The tubes were placed in a pre-cooled glass lyophilizer container and were lyophilized for 48–72 hours. A SPEX SamplePrep 8970 freezer/mill (Metuchen, NJ, https://www.spexsampleprep.com/) was filled with liquid nitrogen. The lyophilized amnion pieces were placed into the freezer/mill chamber. Membrane pieces were milled for 3 cycles of 5 minutes of cool, 5 minutes of mill. Following the grinding, 220 mg of amnion and 22 mg of pepsin (Cat# P7000, Sigma, Darmstadt, Germany, http://www.sigmaaldrich.com) was added into a 15 ml tube. The tube was then gamma irradiated for 1 hour at 1 mega rad. Following gamma radiation, all subsequent steps were performed in sterile conditions. Ten milliliters of sterilized 0.01 N HCl was added to the tube. The materials within the tube were then mixed, allowing digestion for 48 hours at 37°C. The digest was centrifuged at 4,500 rpm for 10 minutes. The supernatant was removed and placed in another 15 ml tube. The solution was neutralized with NaOH to a pH of 7. The amnion solution is referred to as Solubilized Amnion Membrane (SAM) from herein. SAM was stored in aliquots at $-80°C$ until further use. An overview of this process is show in in Figure 1A.

Preparation of HA-SAM Hydrogel

Figure 1B provides a diagram demonstrating the chemistry by which the HA hydrogel is formed using thiol-ene photopolymerization chemistry. HyStem-HP hydrogel (ESI-BIO, Alameda, CA, http://www.esibio.com/) components were dissolved in sterile water. Briefly, heprasil (thiolated HA with conjugated heparin groups) or glycosil (thiolated HA) and Gelin-S (thiolated gelatin) were dissolved in water containing 0.05% (wt/vol) 2-hydroxy-4′-(2-hydroxyethoxy)−2-methylpropiophenone photoinitiator (Sigma, St. Louis, MO) to make 1% (wt/vol) solutions. Extralink, a PEGDA cross-linker, was dissolved in water containing the photoinitiator to make a 2% (wt/vol) solution. Heprasil, Gelin-S, and extralink were then mixed in a 2:2:1 ratio by volume, and SAM solution was incorporated into the HA hydrogel solution at a 1:1 ratio prior UV cross-linking. For cross-linking, HA-SAM hydrogels were irradiated with UV light (365 nm, 18 W/cm^2) at a distance of 3 cm to initiate a thiol–ene stepwise cross-linking reaction.
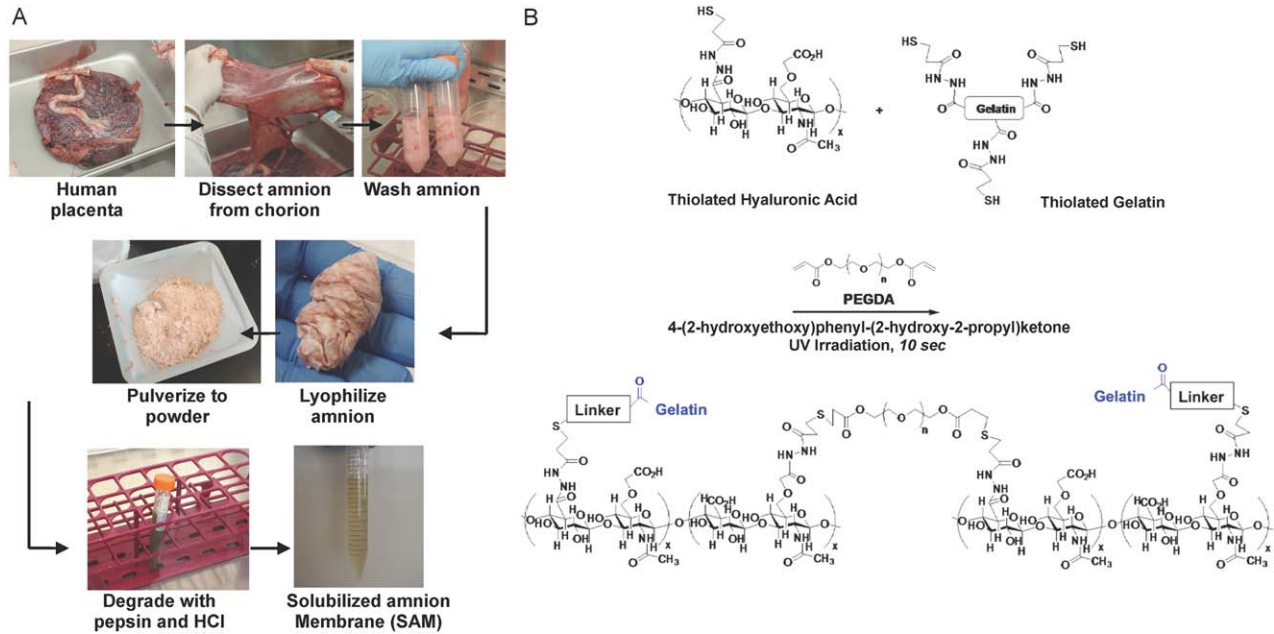
Figure 1. Formulation of Solubilized Amnion Membrane Hydrogel. **(A):** Process of generating solubilized amnion membrane from human placental tissue. Amnion membrane is manually dissected from the chorion membrane and washed with sterile saline to remove blood. The membrane is cut into small pieces, washed in saline and sterile water, and lyophilized/freezer milled. This amnion is then digested in pepsin/HCl and the supernatant is collected. **(B):** A diagram demonstrating the reaction by which the HA-based Extracel hydrogel is formed by thiol-ene photopolymerization chemistry. Thiolated HA and gelatin are cross-linked with PEGDA in the presence of the photoinitiator 4-(2-hydrox-yethoxy)phenyl-(2-hydroxy-2-propyl)ketone using irradiation with UV light. Abbreviations: HA, hyaluronic acid; PEGDA, polyethylene glycol diacrylate.

Hydrogel Swelling Assay

For the hydrogel swelling assay a 500 μl aliquot of HA-SAM or HA alone (water used in place of SAM volume) was gelled in the bottom of replicate glass vials and the vials weighed. Then, 3 ml of Phosphate Buffered Saline (PBS) was added on top of each gel, and the vials were placed into a standard tissue culture incubator at 37°C with 5% CO$_2$. In this case, the hydrogel swelling occurred uniaxially toward the upper direction of the vials. The PBS was changed every hour for 4 hours, after which the vials were weighed after carefully removing the surface PBS. The mass of the both the initially formed and swollen hydrogels was calculated by subtracting the mass of the vial from the total mass. The swelling ratio was defined as a ratio of the mass of the swollen hydrogel divided by the mass of the initially formed hydrogel.

Protein Release Assay

HA-SAM hydrogels were prepared as described above. The gels had a total volume of 500 μl and were prepared in 9 wells of a 24-well plate. Five hundred microliters of PBS were added to the top of each hydrogel, and this volume was collected and replaced after 24 hours and daily for 15 days. The collected liquid was stored at −20°C until the Protein Assay (Bio-Rad, DC Protein Assay Kit II, 500-0112, Hercules, California, http://www.bio-rad.com/) was performed. The resulting data from above were converted into cumulative protein released and plotted versus time. To model the kinetics of the protein release, three release models were applied to the data to achieve a best fitting model as previously described [32] Initially, a simple first-order release kinetic model was applied to the cumulative protein release data set. First-order release rates are described by the following equation:

$$\log Q_t = K \cdot t$$

where Q_t is the cumulative amount of material released at time t, K is the first order release constant, and t is the time in days during the release study. Next, the Hixson–Crowell release kinetic model was applied to the data set. Hixson–Crowell release kinetics are described by

$$\sqrt[3]{Q_t} = K_{HC} \cdot t$$

where, again, Q_t is the cumulative amount of material released at time t, K_{HC} is the Hixson–Crowell release constant, and t is the time in days during the release study. In this model, the application of the cube root describes release that is impacted by changes to the surface area or volume of the container (the hydrogel) by degradation or dissolution. Last, the Higuchi release model was applied to the data. Higuchi release kinetics are described by

$$Q_t = K_H \cdot \sqrt{t}$$

where, once more, Q_t is the cumulative amount of drug released at time t, K_H is the Higuchi release constant, and t is the time in days. In this kinetic model, the cumulative release is plotted against the square root of time, effectively providing a model that describes diffusion of the released protein being governed by the need to travel through the hydrogel polymer matrix.

Human Dermal Fibroblast and Keratinocyte Culture

Human dermal fibroblasts were obtained from human foreskin (ScienCell, Carlsbad, CA, www.sciencellonline.com) and cultured in

High Glucose Dulbecco's modified Eagle's medium (ThermoFisher Scientific, Waltham, MA, http://www.thermofisher.com) supplemented with 5% fetal bovine serum and 1% penicillin/streptomycin (P/S) solution. Human epidermal keratinocytes were also purchased from ScienCell and cultured in keratinocyte serum-free media (Gibco-BRL) supplemented with prequalified human recombinant Epidermal Growth Factor 1-53 (EGF 1-53), Bovine Pituitary Extract, and 1% P/S solution. When sufficient cell numbers were reached in culture, fibroblasts (passage 8–12) and keratinocytes (passage 6–10) were trypsinized for 5 minutes, counted and used for experiments.

Cell Viability Assay

To assess the effects of hydrogel formation and exposure on cell viability, LIVE/DEAD assays were performed on HA, HA-SAM, and collagen encapsulated human keratinocytes and dermal fibroblasts. Cell viability was assessed with the LIVE/DEAD Viability/Cytotoxicity Kit (ThermoFisher Scientific, Waltham, MA, http://www.thermofisher.com). Human keratinocytes and dermal fibroblasts were expanded on two-dimensional tissue culture plates prior to gel encapsulation. The cells were treated with trypsin and counted before centrifugation, after which the supernatant was removed and discarded. The cells were resuspended in the hydrogels at a density of 1×10^6 cells per milliliter of gel. The hydrogel plus cells was irradiated with UV light (365 nm, 18 W/cm²) at a distance of 3 cm for 15–20 seconds for a 500 µl final volume of the hydrogel. Control groups included cells resuspended in a HA hydrogel not containing SAM and a collagen hydrogel. Type I rat tail collagen (3.66 mg/ml, BD Biosciences, Bedford, MA, www.bdbiosciences.com) was prepared as per the manufacturer's instructions. Briefly, the collagen solution was mixed with 10X PBS, water, and 1N NaOH resulting in a 1.25 mg/ml collagen solution at pH 7.0. The collagen gel solutions were transferred to an incubator at 37°C to allow hydrophobic cross-linking to occur. Each hydrogel was formed in one well of a two-well chamber slide, imaged using confocal microscopy, and percentage of live to total cells was quantified using ImageJ.

Metabolism/Proliferation Assay

For metabolism/proliferation assays, keratinocytes and dermal fibroblasts were prepared as above, and 50,000 cells were seeded in 50 µl hydrogel per well in 96-well plates containing the previously prepared hydrogel substrates ($n = 3$ per timepoint). Control groups included cells resuspended in a HA hydrogel not containing SAM, and a collagen hydrogel as described above. The plates were then transferred to an incubator (37°C, 5% CO_2), and metabolism was determined using 3-(4,5-dimethylthiazol-2-yl)-5-(3-carboxymethoxyphenyl)-2-(4-sulfophenyl)-2H-tetrazolium (MTS) assay (Promega, Madison, WI, http://www.promega.com) on days 1, 4, and 7 of culture. Aliquots (100 µl) were removed and absorbance readings determined at 490 nm on the plate reader. Absorbance levels are approximately proportional to the number of live cells. It should be noted that media was not changed during the time course of the MTS assay.

Growth Factor and Cytokine Content Analysis

SAM was prepared as described above and analyzed for growth factor and cytokine content using a Quantibody Human Growth Factor Array (Ray-Biotech, Norcross, GA, http://www.raybiotech.com), an array-based multiplex enzyme-linked immunosorbent assay (ELISA) system for simultaneous quantitative measurement of multiple cytokines, growth factors, proteases, soluble receptors, and other proteins. Analysis was performed by RayBiotech's automated slide processing system.

In Vivo Wound Healing Study

An in vivo wound healing study was performed to evaluate the efficacy of the HA-SAM hydrogel. This study was reviewed and approved by the Wake Forest University Institutional Animal Care and Use Committee. While under anesthesia, a single full-thickness skin wound (2.0×2.0 cm) was surgically created on the mid-dorsal region of nu/nu mice as previously described [33]. Each wounded mouse received one of three treatment options; (a) Untreated other than standard bandaging, (b) HA-gel only, or (c) HA-SAM gel. For all treatments, triple antibiotic (bacitracin zinc, neomycin sulfate, polymyxin-B sulfate; Medique Products, Fort Myers, FL, http://www.mediqueproducts.com) was applied directly to a Tegaderm bandage (3M, St. Paul, MN, http://www.3m.com), which covered the wound after gelation. Finally, a custom-made bandage was sutured in place in order prevent the Tegaderm from being removed. Wound size was documented by taking photographs immediately after surgery and again at 4, 7, 10, and 14 days ($n = 6$), Animals were euthanized at 14 days, and the regenerated skin was harvested for histological analysis.

Wound Closure, Contraction, and Re-Epithelialization

Wound closure, contraction, and re-epithelialization percentages were calculated using photographs and histological examination of the wounds, taken at the time of surgery, and again at 4, 7, 10, and 14 days. Using ImageJ software, the original wound area was defined as A, the clearly re-epithelialized (but thinner) skin area was defined as B, and the remaining unclosed wound was defined as C. Percentage of wound remaining was defined as C/A $\times$ 100%, percentage of contraction of the wound was defined as (A–B)/A $\times$ 100%, and percentage of re-epithelialization was defined as (B–C)/B $\times$ 100%. Wound aspect ratio was also determined to describe observed changes in the shape and direction of wound contraction between groups. Measurements of wound length (head to tail direction) and wound width was measured using Image J, and the length:width ratio determined. Symmetrical contraction result in aspect ratios close to 1, while asymmetrical contraction results in aspect ratios greater than 1.

Histology

Harvested skin tissues were first rolled around a syringe needle to facilitate handling prior to being fixed overnight in 4% paraformaldehyde. Samples were then washed in PBS three times for 30 minutes per wash, after which the samples were transferred to 30% sucrose for an overnight incubation at 4°C. The rolled tissues were then sliced in half and flash frozen in Tissue-Tek OCT Compound (Sakur; Finetek, Torrance, CA, http://www.sakura.com) blocks in liquid nitrogen or processed for paraffin embedding. A cryotome (Leica, Heerbrugg, Switzerland, http://www.leica.com) was used to generate 6-µm frozen sections made up of the entire cross-sections of the regenerating wounds. These slides were stored at −20°C until histological procedures were performed. Sections were stained with H&E for histology, and slides were imaged under light microscopy. Quantification of vascularization was performed by determining the blood vessel density and average vessel size (diameter) H&E-stained wound cross-sections. To do this, ImageJ software was used to perform measurements on histological images. For blood vessel density, first the cross-

sectional area of tissue in the image was determined. Within that area the number of vessels was counted. Blood vessel density values were calculated by dividing the area by the number of vessels, after which the average blood vessel density per group was determined. For average vessel size, vessels were selected at random from histological images taken of each animal. To calculate each individual vessel diameter, the diameter of at least 100 blood vessels was measured using ImageJ and the area approximated using area = πr^2. Areas of each treatment were expressed relative to the average vessel size in healthy, uninjured skin from the same animal. Blood vessel size distribution was also evaluated by grouping vessels into small (<500 μm), medium (500–1,000 μm), or large (>1,000 μm) diameter.

Immunohistochemistry

Immunohistochemical (IHC) staining with smooth muscle actin (SMA) was used to visualize smooth muscle cells in mature blood vessels in the regenerating skin, and with von Willebrand factor (vWF) to visualize endothelial cells in newly formed capillaries and lining the mature blood vessels. For IHC, all incubations were carried out at room temperature unless otherwise stated. Slides were warmed at 60°C for 1 hour to increase bonding to the slides. Antigen retrieval was performed on all slides and achieved with incubation in proteinase K (Dako, Carpinteria, CA, http://www.dako.com) for 5 minutes. Sections were permeabilized with 0.05% Triton X-100 in PBS for 5 minutes. Nonspecific antibody binding was minimized by incubating sections for 10 minutes in Protein Block Solution (Abcam, Cambridge, U.K., http://www.abcam.com). Sections were incubated for 90 minutes in a humidified chamber with the primary anti-SMA (catalog no. A5228, Sigma) and anti-vWF antibodies (catalog no. AB7356; Millipore, Billerica, MA, http://www.millipore.com) at 1:200 dilution in antibody diluent. Following primary incubation, slides were washed three times in PBS for 5 minutes. Sections were then incubated for 60 minutes with Fluorescein Horse Anti-Mouse IgG (FL-2001) secondary antibodies at a 1:25 Dilution and DyLight 594-conjugated AffiniPure donkey anti-rabbit IgG secondary antibodies in a 1:200 dilution in Mouse on Mouse (M.O.M.) Immunodetection reagent (BMK-2202, Vector Laboratories). The sections were washed in PBS, counterstained with 4′,6-diamidino-2-phenylindole (DAPI), and coverslipped with Prolong Gold Antifade (invitrogen, Carlsbad, CA, http://www.invitrogen.com). For Keratin 10 and Ki67 IHC, tissues were treated as described above, but with primary antibodies anti-Keratin 10 antibody (catalog no. PRB-159P, Covance) and anti Ki67 (catalog no. M7249, Dako) and secondary antibodies Invitrogen 488 anti-rabbit IgG and Invitrogen 594 Anti-rat IgG respectively. Native skin samples were harvested as positive controls and were used for comparison. Negative controls were set up at the same time as the primary antibody incubations and included incubation with PBS in place of the primary antibody. No immunoreactivity was observed in these negative control sections. Ki67 positive cells were counted in representative slides for each animal and expressed as a number per field of view for all groups.

Statistical Analysis

Data were expressed for each experimental group as mean ± SD and statistical significance determined using statistical analysis software (GraphPad Prism, Graphpad Software Inc.). Data were analyzed using the repeated measures Analysis of Variance (ANOVA) with the Bonferroni post hoc test. Student's t tests were performed to compare the means of a normally distributed interval dependent variable for two independent groups. Confidence intervals of 95% were assumed to be significant.

Evaluation of Hydrogel Swelling

HA and HA-SAM hydrogels were prepared as described in Figure 1. As previously described [25], the HA-only hydrogels were cross-linked with a 18 w/cm² 365 nm UV lamp at a distance of 3 cm cross-linked in approximately 18–20 seconds. The addition of SAM to the hydrogel had no effect on these cross-linking properties of the biomechanical properties of the hydrogel (data not shown). We next evaluated the swelling properties of the HA-only hydrogel and the HA-SAM. To measure swelling or contraction, each hydrogel was prepared as described above and supplemented with PBS. The hydrogels were weighed upon gelation and every hour for 4 hours until at an equilibrium point 24 hours afterward. The swelling ratio was defined as a ratio of the mass of swollen hydrogel to the mass at equilibrium. The inclusion of SAM increased the swelling ratio from approximately 1.05 to 1.17 over the first 4-hour time-point, which remained stable until the equilibrium 24-hour time-point (Supporting Information Fig. S1A). This difference may be contributed to the significant mass of SAM protein impairing the same degree of cross-linking density in the SAM-free hydrogels, resulting in a looser polymer network, which subsequently is capable of expanding further. However, this difference is quite minor compared with that of different hydrogel formulations with similar applications, where the swelling ratio can range from −0.5 to 2.5 [25], so the significance of this finding is not clear.

Protein Release Kinetics

Cumulative protein release curves were generated from the quantification of protein released daily from HA-SAM hydrogels (Supporting Information Fig. S1B) over a 14-day time-course. As previously described for release of stem cell-derived proteins [33], the majority of the total SAM protein release occurred within the first week, after which cumulative release plateaued, but maintained a minor daily increase. Hydrogel release mechanisms were assessed using with a set of three kinetic mathematical models. Quantification of modeling was important to verify that the general mechanism of release of growth factors from our material was in line with the actual designed hydrogel system components. The models were compared using the R^2 values generated regression lines fitting the data. The three kinetic mathematical models are shown in (Supporting Information Fig. S1C–1E). R^2 values indicated that the Higuchi diffusion-mediated release model was the most accurate for protein release (R^2 of .81365). This is expected, as secreted proteins such as growth factors would be required to diffuse through the polymer network to reach the fluid outside of the hydrogel.

Cell Encapsulation, Viability, and Proliferation

To confirm the biocompatibility of UV-induced cross-linking with HA-SAM, we performed LIVE:DEAD staining of encapsulated keratinocytes and dermal fibroblasts immediately after gel encapsulation and cross-linking. As with all in vitro assays, we performed these studies in triplicate, with three independently derived HA-SAM preparations. We did not measure any significant difference in viability of keratinocytes maintained in HA hydrogel only (97.38% ± 0.26% viable), HA-SAM (95.2% ± 2.74% viable), and collagen hydrogel (98.49% ± 0.12% viable; Fig. 2A). Similarly, no
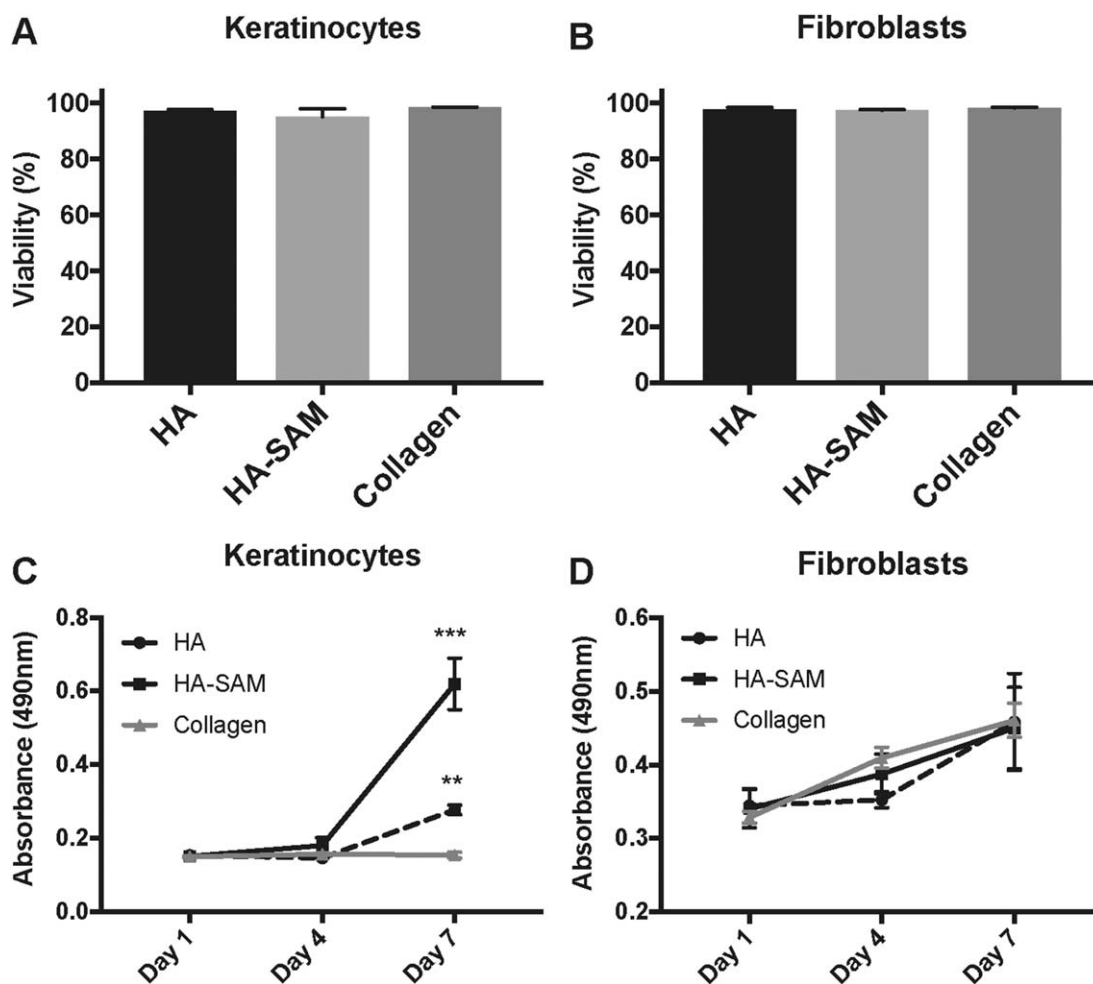
Figure 2. Cell Viability and Proliferation with HA-SAM hydrogel. Demonstration of post-encapsulation viability of primary keratinocytes **(A)** and fibroblasts **(B)** following encapsulation in HA only, HA-SAM hydrogels (cross-linked with UV light) or collagen hydrogels (hydrophobic cross-linking). Cells remained highly viable (95%–99%) following gel encapsulation. **(C):** Keratinocytes maintained in HA-SAM, showed significantly greater absorbance at day 7 than cells maintained in either HA hydrogel only or collagen hydrogel. **(D):** No differences were observed at any time-point for fibroblasts maintained under each of the three conditions, with all groups showing a steady increase in absorbance over time. (**, $p < .001$; ***, $p < .0001$). Abbreviations: HA, hyaluronic acid; SAM, solubilized amnion membrane.

differences in viability were observed for dermal fibroblasts maintained in HA hydrogel only (97.72% ± 0.72% viable), HA-SAM (97.44% ± 0.26% viable), and collagen hydrogel (98.44% ± 0.13% viable; Fig. 2B). An MTS cell metabolism assay was performed as a measure of cell proliferation within each of the hydrogel conditions following a period of culture in vitro. Keratinocytes maintained under the three conditions did not show any significant differences between groups at day 1 or day 4 (Fig. 2C). However, by day 7, keratinocytes maintained in HA-SAM, showed significantly greater absorbance (0.62 ± 0.12) than cells maintained in either HA hydrogel only (0.28 ± 0.02) or collagen hydrogel (0.15 ± 0.01; $p < .0001$). Interestingly, there was also significantly greater absorbance in HA hydrogel compared with collagen hydrogel only ($p < .001$). No differences were observed at any time-point for fibroblasts maintained under each of the three conditions, with all groups showing a steady increase in absorbance over time (Fig. 2D).

Growth Factor and Cytokine Analysis

SAM was prepared as described above and analyzed for growth factor and cytokine content using a Quantibody Human Growth

Factor Array. Proteomics analysis of SAM demonstrated a large range of growth factors and cytokines able to be captured by this assay (Supporting Information Table S1). Of note, SAM contained high concentrations of bone morphogenetic protein 5 (BMP5; 6088.6 pg/ml), bone morphogenetic protein 7 (BMP7; 3645.4 pg/ml), epidermal growth factor receptor (EGF-R; 31219.8 pg/ml), fibroblast growth factor 4 (FGF4; 17213.3 pg/ml), hepatocyte growth factor (HGF; 26791.1 pg/ml), Insulin-like growth factor binding protein (IGFBP1-6; 5871.4–70255.2 pg/ml), Placental Growth Factor-1 (PlGF; 2522.1 pg/ml), transforming growth factor beta 1 (TGFβ1; 5090.8 pg/ml), vascular endothelial growth factor (VEGF; 9681.0 pg/ml), and vascular endothelial growth factor receptor 2 (VEGF R2; 2799.6 pg/ml).

Wound Treatment and Gross Morphology

Both HA-SAM and HA hydrogel only were easy to apply to wounds and resulted in immediate wound coverage. Exposure of the hydrogel to UV light during application resulted in only minimal material flow, which allowed it to conform to the wound shape and depth, but without material loss from the wound area. The rapid cross-linking of the hydrogel provided an ideal delivery
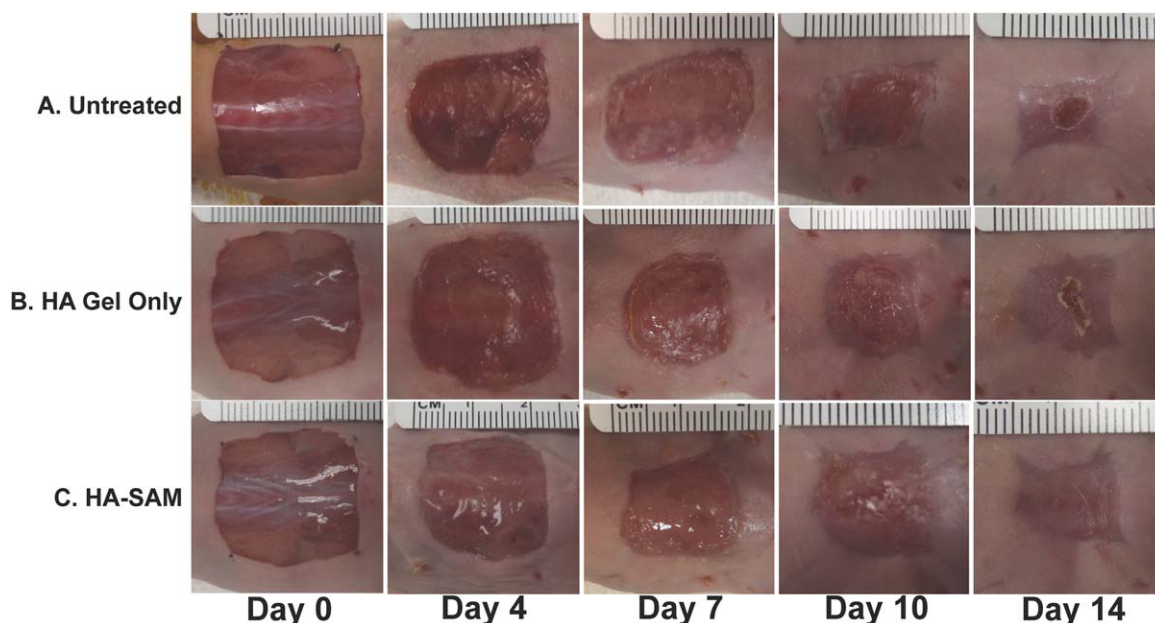
Figure 3. Time-course images from in vivo wound healing study. A 2 × 2 cm full-thickness wound was created on the back of nude mice and received one of three treatment options; **(A):** Untreated other than standard bandaging; **(B):** HA-gel only or; **(C):** HA-SAM hydrogel. Gross morphology demonstrates accelerated wound closure time, increased epithelialization, and reduced contraction in HA-SAM groups. Abbreviations: HA, hyaluronic acid; SAM, solubilized amnion membrane.

system for the full thickness wounds, which followed the natural curve of the mouse dorsum. The applied hydrogels were soft, but robust enough to maintain wound coverage during the bandaging process. The hydrogel was still present four days after application for both the HA-SAM and HA only-treated wounds. By day 7, this appeared as more of a thin transparent film or membrane. It was not clear whether this represented remaining hydrogel, endogenous cellular coverage, or a combination of both (Fig. 3). Untreated wounds remained open during both of these time points. By day 10, the presence of hydrogel within the wound areas was no longer observed and instead replaced by the formation of primarily epithelium in the HA-SAM-treated wounds, and a combination of epithelium, dried scab tissue, and open wound area in the HA only and untreated wounds.

Wound Closure

Wound closure was calculated and expressed as the percentage of wound remaining using photographs taken at the time of surgery and again at 4, 7, 10, and 14 days (Fig. 4A). All groups started at day 0 with 100% wound remaining. At all time-points HA-SAM-treated wounds showed significantly less wound remaining compared with both HA only-treated wounds and untreated wounds ($p < .05$). Specifically at day 4, HA-SAM-treated wounds had $60.84\% \pm 5.08\%$ wound remaining, while HA only-treated wounds showed $80.85\% \pm 3.20\%$ and untreated wounds $81.12\% \pm 12.96\%$ ($p < .01$). The trend toward accelerated wound closure in HA-SAM-treated wounds was maintained at day 7 (HA-SAM: $34.37\% \pm 7.23\%$, HA: $48.25\% \pm 4.92\%$, Untreated: $47.27\% \pm 10.27\%$, $p < .05$), and at day 10 (HA-SAM: $5.27\% \pm 2.11\%$, HA: $20.47\% \pm 4.2\%$, Untreated: $15.34\% \pm 5.13\%$, $p < .01$). By day 14, the differences between groups had narrowed, due to all wounds trending toward complete wound closure. However, HA-SAM-treated wounds still showed significantly less wound remaining compared with the other groups, primarily due to multiple wounds within the group showing complete closure, while

open wound areas still remained in all of the HA-treated and untreated wounds (HA-SAM: $0.13\% \pm 0.15\%$, HA: $3.31\% \pm 1.11\%$, Untreated: $3.69\% \pm 2.54\%$, $p < .05$). There were no significant differences between HA only-treated wounds and untreated wounds at any of the time-points.

Re-Epithelialization

The percentage of wound re-epithelialization was calculated and expressed as the percentage of epithelial covering of the total wounded area at each time-point (Fig. 4B). All groups started at day 0 with 0% wound re-epithelialization. HA-SAM-treated wounds showed significantly more re-epithelialization at each time-point compared with both HA only-treated wounds and untreated wounds ($p < .05$). Specifically at day 4, HA-SAM-treated wounds had $18.45\% \pm 3.68\%$ wound re-epithelialization, while HA only wounds showed $7.14\% \pm 4.40\%$ and untreated wounds showed no signs of re-epithelialization for any wounds the group ($p < .001$). There were also significant differences at day 7 (HA-SAM: $32.72\% \pm 10.62\%$, HA: $16.62\% \pm 8.15\%$, Untreated: $3.38\% \pm 4.14\%$, $p < .05$), and at day 10 (HA-SAM: $82.15\% \pm 7.23\%$, HA: $37.79\% \pm 9.91\%$, Untreated: $29.63\% \pm 3.36\%$, $p < .0001$). All three groups showed significant differences to each other at day 14, with HA-SAM-treated wounds trending toward 100% wound re-epithelialization at this final time-point (HA-SAM: $99.34\% \pm 0.72\%$, HA: $84.86\% \pm 3.34\%$, Untreated: $65.69\% \pm 18.07\%$, $p < .001$). Interestingly, there also seemed like HA hydrogel itself may have a role in promoting re-epithelialization, showing a slight improvement over untreated wounds at day 4 and day 14 ($p < .05$). However, no clear trend over the entire time course of the experiment was observed.

Wound Contraction

Wound contraction was calculated and expressed in two ways. First, expressed as a percentage of the total regenerated/wounded area over the original total wound area (Fig. 4C) and second, the wound aspect ratio of the wound length:width (Fig.
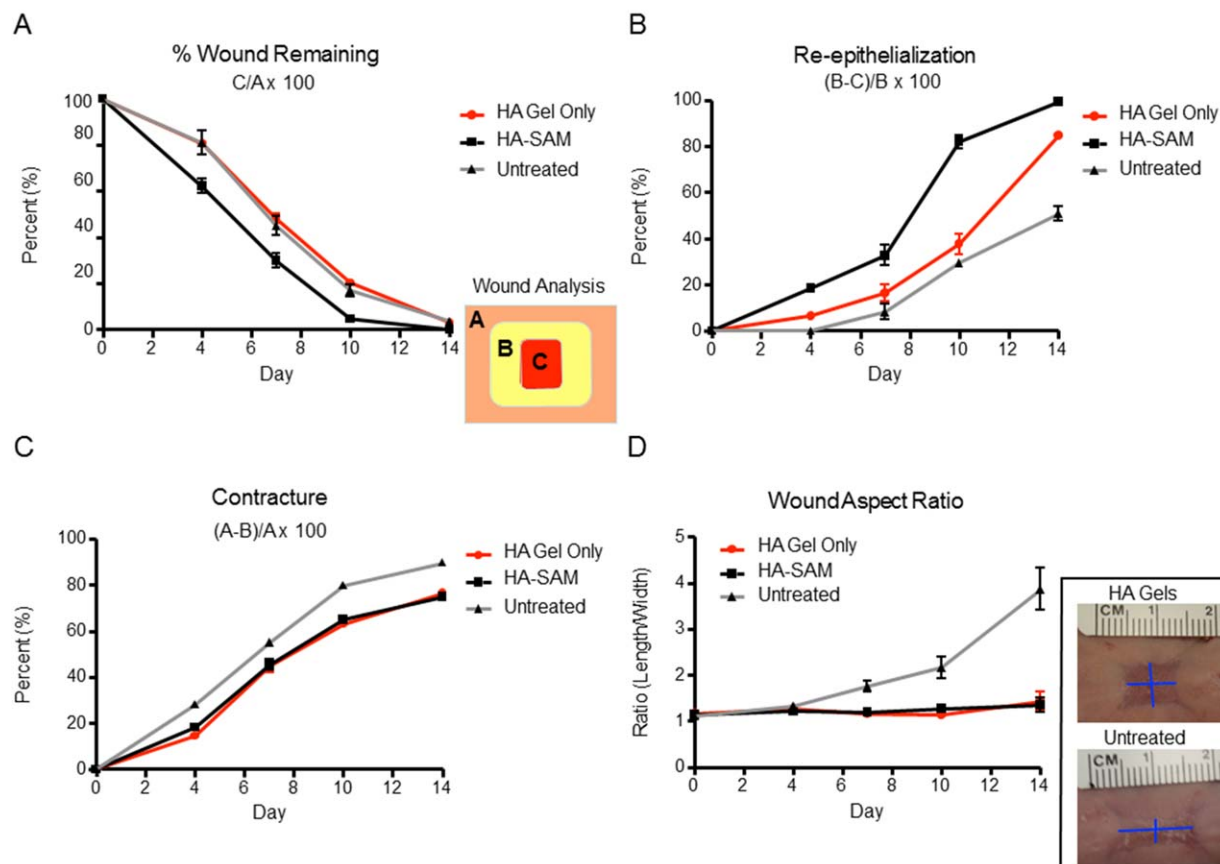
Figure 4. Quantitative Analysis of Wound Healing. **(A):** Percentage (%) wound remaining was calculated by dividing the area of the remaining wound by the original wound size (C/A × 100). HA-SAM groups had significant acceleration of wound closure times resulting in wound closure 3–4 days before other groups. **(B):** Wound re-epithelialization was calculated by measuring newly re-epithelized skin, taking into consideration remaining wound area and contraction ([B-C]/B × 100). HA-SAM groups had significantly greater wound re-epithelialization at all time-points compared with other groups. **(C):** Contraction was measured based on original wound size and the area of re-epithelized skin ([A-B]/A × 100). HA only and HA-SAM groups had significantly less contraction compared with untreated animals. **(D):** Wound aspect ratio was determined to describe observed changes in the shape and direction of wound contraction between groups (length:width). HA only and HA-SAM groups displayed symmetrical contraction, with aspect ratios close to 1, while other groups showed asymmetrical contraction with aspect ratios closer to 4.

4D). These two measurements of wound contraction represent two common characteristics of wound contraction, the shrinking of total wound area and the distortion of wound shape. All groups started at day 0 with 0% wound contraction. Over all time-points, there appeared to be a clear trend of untreated wounds showing greater contraction compared with HA-SAM-treated wounds and HA only-treated wounds. At day 4, HA only-treated wounds showed a slight, but significant decrease in wound contraction compared with HA-SAM-treated wounds and untreated wounds (HA-SAM: $21.19\% \pm 5.79\%$, HA: $13.45\% \pm 1.75\%$, Untreated: $26.52\% \pm 3.35\%$, $p < .05$). However, this trend was not observed at subsequent time-points, with both HA-SAM and HA only-treated wounds both showing significant differences to untreated wounds ($p < .05$), but not each other. This difference was maintained at day 7 (HA-SAM: $48.61\% \pm 7.27\%$, HA: $44.90\% \pm 5.96\%$, Untreated: $54.48\% \pm 1.93\%$, $p < .05$), day 10 (HA-SAM: $70.75\% \pm 1.613\%$, HA: $66.68\% \pm 6.56\%$, Untreated: $80.04\% \pm 1.18\%$, $p < .01$), and day 14 (HA-SAM: $77.90\% \pm 4.23\%$, HA: $78.58\% \pm 2.93\%$, Untreated: $88.20\% \pm 3.43\%$, $p < .01$).

The wound aspect ratio ranged from 1, representing a wound with even length:width, to 4, representing a wound with a length 4 times as long as it's width. There were no significant differences between day 0 and day 4 of analysis, suggesting that while wounds did contract, it occurred with equal effect along each of the measured dimensions. However, beginning at day 7 and continuing until the final time-point, untreated wounds showed a significant increase in the wound aspect ratio compared with the HA-SAM and HA only-treated wounds, both of which remained close to 1. Specifically, the wound aspect ratio was calculated at day 7 (HA-SAM: 1.19 ± 0.12, HA: 1.16 ± 0.12, Untreated: 1.76 ± 0.29, $p < .001$), at day 10 (HA-SAM: 1.27 ± 0.19, HA: 1.14 ± 0.13, Untreated: 2.17 ± 0.59, $p < .01$), and day 14 (HA-SAM: 1.35 ± 0.38, HA: 1.43 ± 0.49, Untreated: 3.53 ± 1.22, $p < .01$).

Gross Histology and Tissue Thickness

Evaluation of the overall wound area was performed by compiling a series of >50 individual images into a single image using ImageJ's image stitching capabilities. This visual allowed us to appreciate the total wound area, size, thickness, epidermis and dermis formation (data not shown), as well as for higher resolution and quantitative analysis. Untreated wounds (Fig. 5A) appeared to have a thinner regenerated wound area compared
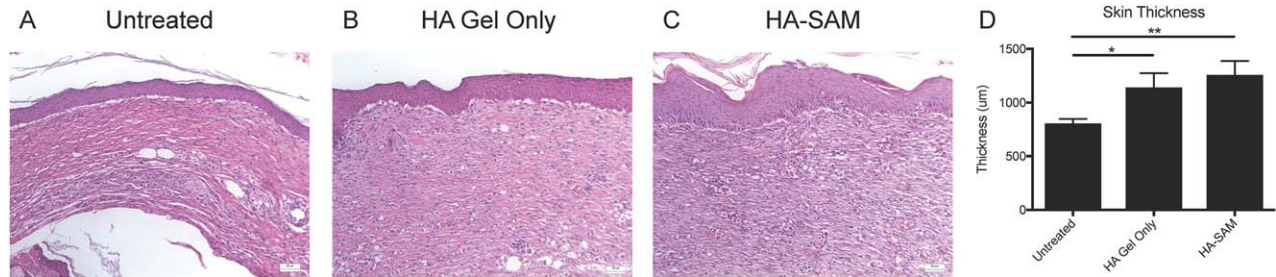
Figure 5. Histological Analysis of Wound Healing. High magnification H&E stained sections showing epidermis formation and dermis composition of untreated **(A)**, HA only **(B),** or HA-SAM-treated **(C)** skin. **(D):** Total skin thickness measurements showed an increased thickness of HA only and HA-SAM-treated skin compared with untreated wounds. (*, $p < .01$; **, $p < .001$). Abbreviations: HA, hyaluronic acid; SAM, solubilized amnion membrane.

with HA-SAM (Fig. 5B) or HA only-treated wounds (Fig. 5C). This was quantified using total skin thickness measurements on high magnification images, showing an increased thickness of HA-SAM-treated skin (1259 ± 315.3 μm, $p < .01$) and HA-gel only (1142 ± 326.1 μm, $p < .05$) compared with untreated wounds (804.2 ± 104.9 μm). Presence of rete pegs or hair follicles was not observed in the central wound area, although some were observed toward the wound edge, likely due to migration and regeneration of endogenous cells.

Blood Vessel Density, Size, and Size Distribution

Quantification of blood vessel density was performed by counting the number of blood vessels in representative high-resolution microscopy images, expressed relative to the cross-sectional area of tissue in the image. Representative images are shown in Figure 6A–6C. HA-SAM-treated wounds showed a significantly greater number of blood vessels per measured area (4.03 ± 0.62) compared with HA only-treated (2.64 ± 0.42, $p < .01$) and untreated wounds (2.03 ± 0.57, $p < .001$; Fig. 6D). To determine the average blood vessel size, ImageJ was used to measure the vessel diameter of at least 100 vessels per sample, and the area approximated using area $= \pi r^2$. To control for any inaccuracies in assuming circular blood vessel presentation in histological sections, data were expressed relative to vessel size measured in healthy, uninjured skin from the same animal. Interestingly, HA-SAM-treated wounds showed an overall smaller average vessel area (0.59 ± 0.23) compared to HA only-treated (0.96 ± 0.19, $p < .05$) and untreated wounds (1.06 ± 0.21, $p < .01$; Fig. 6E). To understand why we were observing an increase in vessel number, but a decrease in average vessel size, we analyzed our data to visualize vessel size distribution by grouping vessels into either small (<500 μm), medium (500–$1,000$ μm) or large ($>1,000$ μm) diameter. The need to control for potential bias due to histological artifacts was not required for this assay, which involved comparison between vessel groupings and not specific size values. This data demonstrated that HA-SAM-treated wounds had similar density of large or medium sized blood vessels, but significantly greater density of small blood vessels (299.3 ± 19.57) compared with HA only-treated (180.6 ± 16.64, $p < .01$) and untreated wounds (159.28 ± 14.53, $p < .0001$). Overall average blood vessel size was significantly smaller in HA-SAM-treated animal compared with HA-gel only and untreated groups, which appeared to be due to a larger number of small vessels and equal numbers of large and medium vessels in the regenerated wound tissue.

IHC staining was performed for α-smooth muscle actin (αSMA) to visualize smooth muscle cells in mature blood vessels in the regenerating skin together with vWF to visualize endothelial cells in newly formed capillaries and lining the mature blood vessels. Compared with untreated (Fig. 6G) and HA only-treated wounds (Fig. 6H), HA-SAM-treated wounds (Fig. 6I) appeared to show significantly more vWF positive blood vessels and these blood vessels appeared smaller in size than vessels within skin from other groups, matching our quantitative evaluation. Slightly more αSMA positive blood vessels were also observed in HA-SAM-treated wounds, but these large αSMA positive blood vessels were too sparse to provide the power sufficient for comparison. IHC staining for keratin 10 was performed to distinguish the epidermis from the dermis together with Ki-67 to visualize proliferating cells within the tissues (Fig. 7A–7C). In HA-SAM and HA-only-treated wounds, proliferating cells were identified in the basal layer of the epidermis of the regenerating wounds. In untreated groups proliferating cells were mostly identified within the dermis, while these were rare in HA only and HA-SAM groups. We observed significantly more proliferating cells in HA-SAM-treated animals (27.38 ± 2.41 per field of view) compared with HA-only-treated (10.95 ± 1.86 per field of view, $p < .0001$) and untreated groups (12.6 ± 3.30 per field of view, $p < .0001$; Fig. 7D).

DISCUSSION

Chronic, large, or nonhealing wounds are a major source of patient mortality and morbidity, as well as representing a significant financial burden on our health care system. The early closure and protection of wounds is vital to increase patient survivability and recovery. However, the current wound coverings available have significant limitations, including the requirement for secondary biopsy sites for harvesting of autologous split-thickness grafts, immune rejection of allogeneic grafts, and excessive costs for biological skin substitutes. To overcome these limitations, we developed a biological wound-healing product, derived from a solubilized human amnion membrane incorporated into a HA hydrogel. This product has not been decellularized, thus while not containing live cells, our manufacturing process preserves the cellular and extracellular components of the amnion. It has been demonstrated that the amnion contains cell populations with potentially therapeutic properties [34, 35], and that the lyophilization of these cells and tissues does not alter their wound treatment efficacy. Extensive studies have confirmed the effectiveness of amnion prepared by lyophilization produces a wound dressing that is safe and effective for promoting wound healing and preventing wound infection [8, 24, 36–38].

Hydrogels and other gel-like wound dressings have recently found clinical application for burn and wound dressings, as they
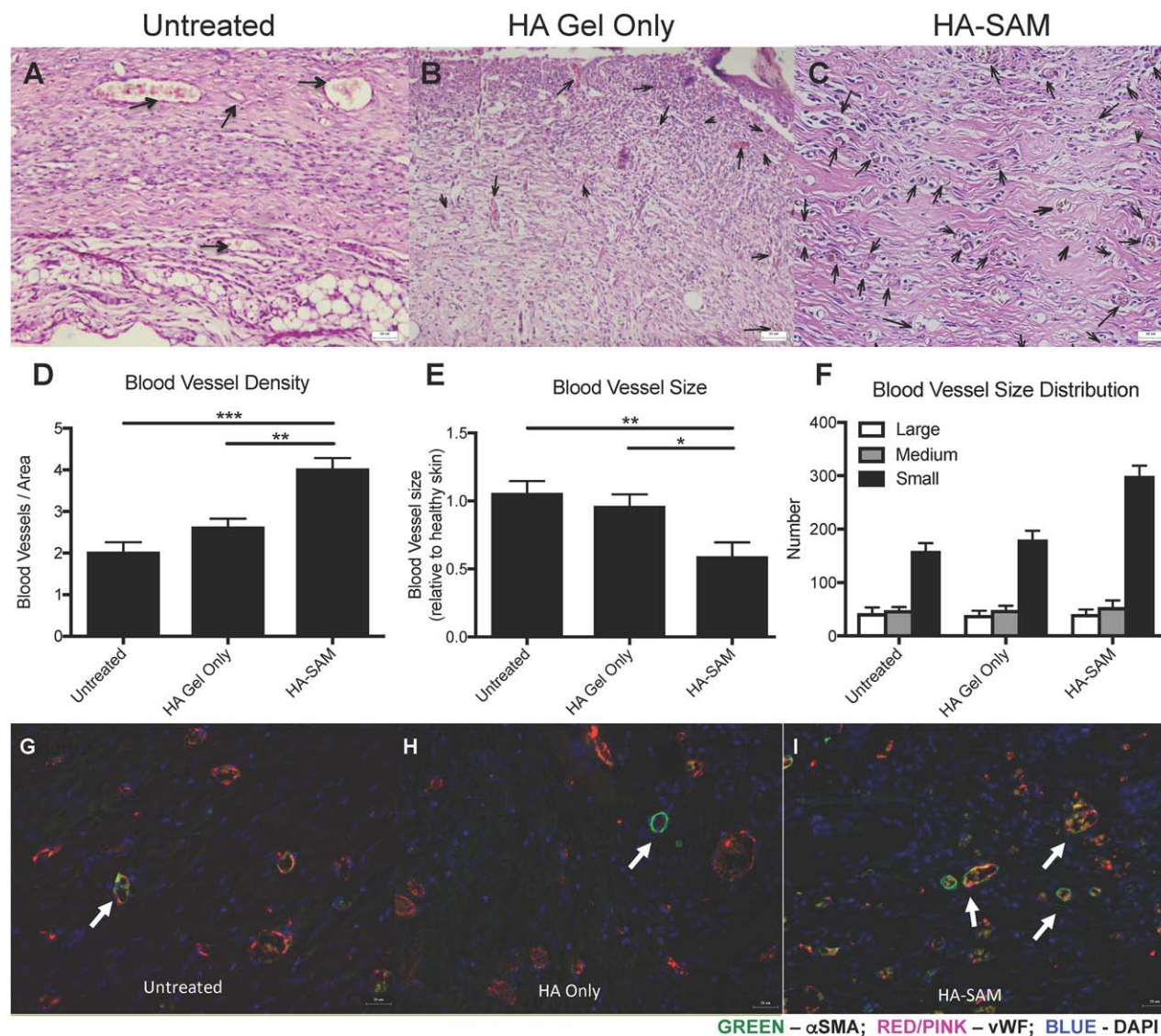
Figure 6. Blood Vessel Formation in Healing Wounds. H&E stained sections of wound area demonstrating blood vessels within the newly regenerated untreated (arrows) **(A)**, HA only **(B)**, or HA-SAM-treated **(C)** skin. **(D):** Blood vessel density within areas of regenerated skin. There were significantly more blood vessels in HA-SAM-treated animal compared to HA only and untreated groups. Counts were performed on six representative fields of view. **(E):** Blood vessel area was calculated and represented as relative to blood vessel size within healthy skin of the same mouse. Average blood vessel size was significantly smaller in HA-SAM-treated animal compared to HA only and untreated groups. **(F):** HA-SAM-treated wounds had similar density of large or medium sized blood vessels, but significantly greater density of small blood vessels compared to HA only-treated and untreated wounds. Immuno-fluorescent staining for αSMA and vWF to stain for blood vessels in the regenerating skin of untreated **(G)**, HA only **(H)**, and HA-SAM **(I)** animals. HA-SAM samples had significantly more blood vessels than other groups. These blood vessels also appeared smaller in size than vessels within skin from other groups. Scale bars = 50 μm (A–C) Scale bars = 25 μm (G–I). (*, $p < .05$; **, $p < .01$; ***, $p < .01$). Abbreviations: αSMA, α-smooth muscle actin; DAPI, 4',6-diamidino-2-phenylindole; HA, hyaluronic acid; SAM, solubilized amnion membrane; vWF, von Willebrand factor.

show superior wound coverage to traditional dry dressings, and are effective in retaining and creating a moist environment within the wound to facilitate wound healing. Current hydrogel dressings are applied either as an amorphous gel or as a pre-formed sheet or film. Some examples such as Nu-gel (sodium alginate, Johnson & Johnson, Ascot, U.K.), Purilon (sodium carboxymethylcellulose/calcium alginate, Coloplast), and Hyalosafe and Hyalomatrix (HA derivative, Anika Therapeutics s.r.l., Abano Terme, Italy). HA possesses many properties that make it a desirable material for wound healing applications. It is a glycoaminoglycan component of the extracellular matrix naturally occurring within the skin,

cartilage and connective tissues. A recent clinical study has demonstrated that HA-based dressings are effective for managing acute wounds particularly in terms of its safety and efficacy [39]. Additionally, we have recently demonstrated that the commercially available HyStem HA hydrogel, modified to have nearly instantaneous in situ photocross-linking through thiol–ene chemistry, provides an ideal carrier for the delivery of stem cells or cell-derived paracrine factors directly into full thickness excisional wounds [32].

In this study, we aimed to improve the known therapeutic potential of the amnion for wound healing by incorporating
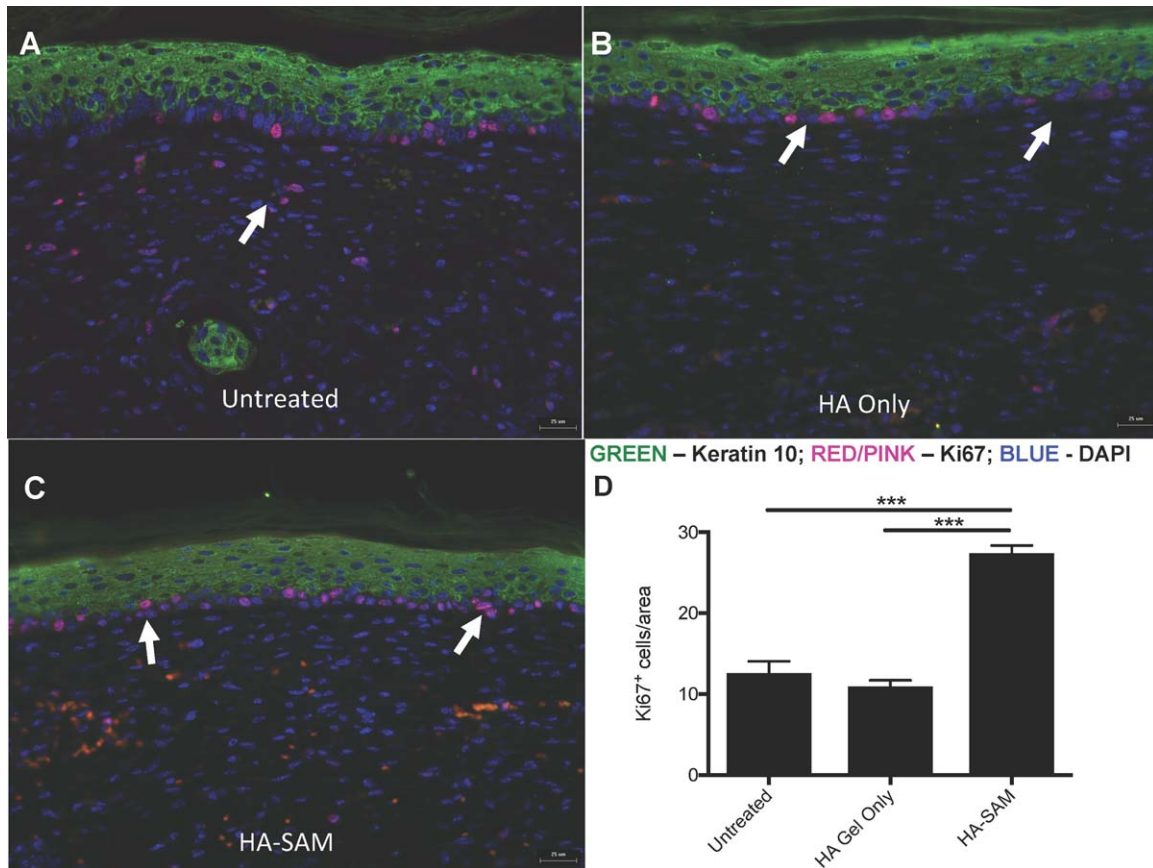
Figure 7. Cell Proliferation in Healing Wounds. Immuno-fluorescent staining for proliferating cells in the epidermis of untreated **(A)**, HA only **(B)**, and HA-SAM **(C)** animals. Antibodies for keratin 10 were used to highlight the epidermis and Ki-67 to stain proliferating cells. More proliferating cells were identified in the basal layer of the epidermis of HA-SAM-treated animals compared to HA-gel only-treated and untreated groups (arrows). In untreated groups proliferating cells were also identified within the dermis, while this was rare in HA only and HA-SAM groups. Significantly more proliferating cells were observed in HA-SAM-treated animals compared to HA-only-treated and untreated groups. Scale bars = 25 μm. (***, $p < .0001$). Abbreviations: DAPI, 4′,6-diamidino-2-phenylindole; HA, hyaluronic acid; SAM, solubilized amnion membrane.

solubilized amnion membrane into a UV-cross-linked HA-based hydrogel. We hypothesized that HA-SAM would be easy to apply to full-thickness wounds, where it would conform to nonuniform wound shape, and that it would significantly improve wound healing through the promotion of re-epithelialization and prevention of wound contraction. We found that the HA hydrogel incorporated SAM within the hydrogel structure, releasing bound proteins via Higuchi diffusion-mediated release. To evaluate the efficacy of HA-SAM as a wound treatment, we used a full-thickness murine wound model, and compared HA-SAM treatment to HA-only and untreated wounds. Morphological analysis demonstrated that HA-SAM significantly accelerated wound closure through re-epithelialization and prevented wound contraction. Histologically, HA-SAM-treated wounds had thicker regenerated skin, increased total number of blood vessels, specifically small and newly formed vessels. Our in vitro observations that HA-SAM was beneficial to keratinocyte proliferation were supported by our in vivo IHC analysis, where we observed greater numbers of proliferating keratinocytes within HA-SAM-treated wounds. Our findings that HA-SAM support the proliferation of keratinocytes in vitro and in vivo, as well as induced the formation of neovascularization, may be explained by the growth factor composition of SAM. While our observations are likely a result of multiple factors, beyond what was evaluated here, the presence of growth factors known to

promote keratinocyte proliferation (bFGF, NGF, HB-EGF) [40] and migration (HGF, IGF1, EGF, FGF-7) [41] would explain some aspects of our presented data. Similarly, growth factors present in SAM known to promote neovascularization (FGF-family, EGF-R, EG-VEGF, VEGF) [42, 43] are likely to have contributed to the observed increase in new blood vessel formation. Overall, this study confirms the efficacy of the amnion membrane as a wound treatment/dressing, and overcomes many of the limitations associated with using fresh, cryopreserved, or dehydrated tissue by providing a hydrogel delivery system for SAM.

The murine nude model of wound injury and regeneration is commonly used for basic research studies and evaluation of potential new therapies. However, there are significant limitations to this model that are well recognized. First, unlike humans, where large acute wounds are unlikely to heal without intervention, the mouse has remarkable endogenous regeneration potential. However, the 14-day wound healing window observed in this study still provides us the opportunity to compare the influence of wound treatments on the rates of epithelialization, wound closure and contraction. While we found significant improvement in these parameters in our mouse model, we anticipate that these improvements would have even greater impact in wounds that are slow to heal. Second, due to the rapid wound closure in the relatively healthy mouse model used in this study, evaluation of

long-term scarring is difficult to perform. The fact that we observed accelerated wound closure, driven primarily by increased epithelialization and reduced contraction, suggests that HA-SAM can be applied to full thickness wounds to promote the formation of healthy regenerated skin. Finally, the use of an immunodeficient nude mouse model, precludes any evaluation of immune-rejection of the human tissue, or conversely, the reported anti-inflammatory and immunomodulatory effects of the amnion membrane. Future studies using large animal models, with or without slow or difficult to heal wounds will be needed to address these questions.

It is also worth discussing the role of the HA hydrogel carrier in the support of wound healing. As discussed previously, there are multiple studies now describing the benefits of HA-based wound dressings for reducing inflammation and promoting wound healing [44–46]. In our study, while the impact of HA treatment was overshadowed by the positive effects of HA-SAM, there were some noticeable improvement in HA-only treated wounds. Specifically, we observed improvements in keratinocyte proliferation in HA hydrogels compared with collagen, and in our mouse model, we observed decreased contraction and increased epithelialization, although this did not have a major impact on wound closure times. Similarly, we observed that HA-treated wounds had thicker regenerated tissue, and slightly greater levels of new blood vessel formation compared with untreated wounds. From these findings, we are able to conclude that HA hydrogel treatment alone also contributes to improved wound healing, although the main improvement occurred when HA hydrogel contained SAM. A major benefit of using a hydrogel such as HA is the potential to selectively modify the hydrogel properties to best match specific applications. We previously developed a modular HA-based hydrogel with different cross-linking approaches that allows for the modification of hydrogel pore size, stiffness and protein/growth factor binding and release characteristics [25, 32]. In our upcoming studies, we plan on evaluating the role of hydrogel stiffness on wound healing, and the potential to match protein/growth factor release to specific wound types. For example, we hypothesize that

a fast releasing hydrogel would be best suited for acute burns or wounds, while a long lasting and slow releasing hydrogel would be more useful for the treatment of slow or difficult to heal wound such as diabetic ulcers.

CONCLUSION

In conclusion, this study demonstrated that HA-SAM maintains the safety and efficacy of amniotic membrane for wound healing, combined with a UV cross-linked HA-hydrogel delivery system for easy application and conformation to full-thickness wounds. Our approach overcomes many of the limitations of living, cellular wound treatments, while still providing biological support for endogenous wound healing mechanisms. Further studies will test the efficacy of HA-SAM in large and/or diseased wound healing animal models, as well as explore the use of multiple administrations, inclusion of biopsy-derived cells or stem cells, and potential delivery using three-dimensional bioprinting technology.

AUTHOR CONTRIBUTIONS

S.V.M. and A.S.: conception and design, collection and/or assembly of data, data analysis and interpretation, manuscript writing, final approval of manuscript; L.S., K.S., and R.H.: collection and/or assembly of data, final approval of manuscript; D.L.M.: conception and design, collection and/or assembly of data; J.J.: conception and design, final approval of manuscript; S.S. and A.A.: conception and design, financial support, final approval of manuscript.

DISCLOSURE OF POTENTIAL CONFLICTS OF INTEREST

S.V.M, A.S., and A.A. have filed patent applications: US20140342015, US20140348940, and EP2897625. All other authors indicated no potential conflicts of interest.

REFERENCES

1 Brigham PA, McLoughlin E. Burn incidence and medical care use in the United States: Estimates, trends, and data sources. J Burn Care Rehabil 1996;17:95–107.

2 Miller SF, Bessey P, Lentz CW et al. National burn repository 2007 report: a synopsis of the 2007 call for data. J Burn Care Res 2008;29:862–870; discussion 871.

3 Beckrich K, Aronovitch SA. Hospital-acquired pressure ulcers: A comparison of costs in medical vs. surgical patients. Nurs Econ 1999;17:263–271.

4 MarketsandMarkets.com. Wound Care Market by Product - MD2611. May 2017. http://www.marketsandmarkets.com/Market-Reports/wound-care-market-371.html

5 Morrow T. Wound healing promoted with living-skin substitutes. Manag Care 2004;13:62–63.

6 Lesher AP, Curry RH, Evans J et al. Effectiveness of Biobrane for treatment of partial-thickness burns in children. J Pediatr Surg 2011;46:1759–1763.

7 Rahmanian-Schwarz A, Beiderwieden A, Willkomm L-M et al. A clinical evaluation of

Biobrane® and Suprathel® in acute burns and reconstructive surgery. Burns 2011;37:1343–1348.

8 John T. Human amniotic membrane transplantation: Past, present, and future. Ophthalmol Clin North Am 2003;16:43–65, vi.

9 Pigeon J. Treatment of second-degree burns with amniotic membranes. Can Med Assoc J 1960;83:844.

10 Cornwell KG, Landsman A, James KS. Extracellular matrix biomaterials for soft tissue repair. Clin Podiatr Med Surg 2009;26:507–523.

11 Bose B. Burn wound dressing with human amniotic membrane. Ann R Coll Surg Engl 1979;61:444–447.

12 Quinby WC, Jr., Hoover HC, Scheflan M et al. Clinical trials of amniotic membranes in burn wound care. Plast Reconstr Surg 1982;70:711–717.

13 Sawhney C. Amniotic membrane as a biological dressing in the management of burns. Burns 1989;15:339–342.

14 Mohammadi AA, Jafari SMS, Kiasat M et al. Effect of fresh human amniotic membrane dressing on graft take in patients with

chronic burn wounds compared with conventional methods. Burns 2013;39:349–353.

15 Branski LK, Herndon DN, Celis MM et al. Amnion in the treatment of pediatric partial-thickness facial burns. Burns 2008;34:393–399.

16 Hermans MH. Preservation methods of allografts and their (lack of) influence on clinical results in partial thickness burns. Burns 2011;37:873–881.

17 Fairbairn N, Randolph M, Redmond R. The clinical applications of human amnion in plastic surgery. J Plast Reconstr Aesthet Surg 2014;67:662–675.

18 Lo K, Kohanim S, Trief D et al. Role of amniotic membrane transplantation in acute chemical injury. Int Ophthalmol Clin 2013;53:33–41.

19 John T. Human amniotic membrane transplantation. Ophthalmol Clin 2003;16:43–65.

20 Fetterolf DE, Snyder RJ. Scientific and clinical support for the use of dehydrated amniotic membrane in wound management. Wounds 2012;24:299–307.

21 Zelen CM, Serena TE, Denoziere G et al. A prospective randomised comparative

parallel study of amniotic membrane wound graft in the management of diabetic foot ulcers. Int Wound J 2013;10:502–507.

22   Zelen C. An evaluation of dehydrated human amniotic membrane allografts in patients with DFUs. J Wound Care 2013;22:347–351.

23   Zelen CM, Serena TE, Fetterolf DE. Dehydrated human amnion/chorion membrane allografts in patients with chronic diabetic foot ulcers: A long-term follow-up study. Wound Med 2014;4:1–4.

24   Bujang-Safawi E, Halim A, Khoo T et al. Dried irradiated human amniotic membrane as a biological dressing for facial burns—A 7-year case series. Burns 2010;36:876–882.

25   Murphy SV, Skardal A, Atala A. Evaluation of hydrogels for bio-printing applications. J Biomed Mater Res Part A 2013;101:272–284.

26   Fraser JR, Laurent TC, Laurent UB. Hyaluronan: Its nature, distribution, functions and turnover. J Intern Med 1997;242:27–33.

27   Toole BP. Hyaluronan in morphogenesis. Semin Cell Dev Biol 2001;12:79–87.

28   Burdick JA, Prestwich GD. Hyaluronic acid hydrogels for biomedical applications. Adv Mater 2011;23:H41–56.

29   Allison DD, Grande-Allen KJ. Review. Hyaluronan: A powerful tissue engineering tool. Tissue Eng 2006;12:2131–2140.

30   Prestwich GD, Kuo JW. Chemically-modified HA for therapy and regenerative medicine. Curr Pharm Biotechnol 2008;9:242–245.

31   Prestwich GD, Shu XZ, Liu Y, Inventors. Modified macromolecules and methods of making and using thereof. PCT/US2004/040726. 2005. http://www.marketsandmarkets.com/Market-Reports/wound-care-market-371.html

32   Skardal A, Murphy SV, Crowell K et al. A tunable hydrogel system for long-term release of cell-secreted cytokines and bioprinted in situ wound cell delivery. J Biomed Mater Res B Appl Biomater 2017;105:1986–2000.

33   Skardal A, Mack D, Kapetanovic E et al. Bioprinted amniotic fluid-derived stem cells accelerate healing of large skin wounds. STEM CELLS TRANSLATIONAL MEDICINE 2012;1:792–802.

34   Murphy SV, Kidyoor A, Reid T et al. Isolation, cryopreservation and culture of human amnion epithelial cells for clinical applications. J Vis Exp 2014.

35   Murphy S, Lim R, Dickinson H et al. Human amnion epithelial cells prevent bleomycin-induced lung injury and preserve lung function. Cell Transplant 2011;20:909–923.

36   Forbes J, Fetterolf D. Dehydrated amniotic membrane allografts for the treatment of chronic wounds: A case series. J Wound Care 2012;21:290–292.

37   Sheikh ES, Sheikh ES, Fetterolf DE. Use of dehydrated human amniotic membrane allografts to promote healing in patients with refractory non healing wounds. Int Wound J 2014;11:711–717.

38   Shah AP. Using amniotic membrane allografts in the treatment of neuropathic foot ulcers. J Am Podiatr Med Assoc 2014;104:198–202.

39   Voinchet V, Vasseur P, Kern J. Efficacy and safety of hyaluronic acid in the management of acute wounds. Am J Clin Dermatol 2006;7:353–357.

40   Mitev V, Miteva L. Signal transduction in keratinocyte proliferation and differentiation. Biomedical Rev 1997;8:73–85.

41   Seeger MA, Paller AS. The roles of growth factors in keratinocyte migration. Adv Wound Care 2015;4:213–224.

42   Brouillet S, Hoffmann P, Feige J-J et al. EG-VEGF: A key endocrine factor in placental development. Trends Endocrinol Metab 2012;23:501–508.

43   Cross MJ, Claesson-Welsh L. FGF and VEGF function in angiogenesis: Signalling pathways, biological responses and therapeutic inhibition. Trends Pharmacol Sci 2001;22:201–207.

44   King S, Hickerson W, Proctor KG. Beneficial actions of exogenous hyaluronic acid on wound healing. Surgery 1991;109:76–84.

45   Weigel P, Frost S, McGary C et al. The role of hyaluronic acid in inflammation and wound healing. Int J Tissue React 1987;10:355–365.

46   Doillon CJ, Silver FH. Collagen-based wound dressing: Effects of hyaluronic acid and firponectin on wound healing. Biomaterials 1986;7:3–8.

See www.StemCellsTM.com for supporting information available online.